

Anomalous anisotropic magnetoresistance in single-crystalline Co/$SrTiO_3$(001) heterostructures

Shuang-Long Yang(杨双龙), De-Zheng Yang(杨德政), Yu Miao(缪宇), Cun-Xu Gao(高存绪), and De-Sheng Xue(薛德胜)

Citation: Chin. Phys. B, 2021, 30 (**12**): 127302. DOI: 10.1088/1674-1056/ac05ad
Journal homepage: http://cpb.iphy.ac.cn; http://iopscience.iop.org/cpb

What follows is a list of articles you may be interested in

Giant Rashba-like spin-orbit splitting with distinct spin texture in two-dimensional heterostructures

Jianbao Zhu(朱健保), Wei Qin(秦维), and Wenguang Zhu(朱文光)
Chin. Phys. B, 2021, 30 (**8**): 087307. DOI: 10.1088/1674-1056/ac0784

Investigation on threshold voltage of p-channel GaN MOSFETs based on p-GaN/AlGaN/GaN heterostructure

Ruo-Han Li(李若晗), Wu-Xiong Fei(费武雄), Rui Tang(唐锐), Zhao-Xi Wu(吴照玺), Chao Duan(段超), Tao Zhang(张涛), Dan Zhu(朱丹), Wei-Hang Zhang(张苇杭), Sheng-Lei Zhao(赵胜雷), Jin-Cheng Zhang(张进成), and Yue Hao(郝跃)
Chin. Phys. B, 2021, 30 (**8**): 087305. DOI: 10.1088/1674-1056/ac0793

High-performance self-powered photodetector based on organic/inorganic hybrid van der Waals heterojunction of rubrene/silicon

Yancai Xu(徐彦彩), Rong Zhou(周荣), Qin Yin(尹钦), Jiao Li(李娇), Guoxiang Si(侣国翔), and Hongbin Zhang(张洪宾)
Chin. Phys. B, 2021, 30 (**7**): 077304. DOI: 10.1088/1674-1056/abf345

Scanning tunneling microscopic investigation on morphology of magnetic Weyl semimetal $YbMnBi_2$

Zhen Zhu(朱朕), Dong Yan(严冬), Xiao-Ang Nie(聂晓昂), Hao-Ke Xu(徐豪科), Xu Yang(杨旭), Dan-Dan Guan(管丹丹), Shiyong Wang(王世勇), Yao-Yi Li(李耀义), Canhua Liu(刘灿华), Jun-Wei Liu(刘军伟), Hui-Xia Luo(罗惠霞), Hao Zheng(郑浩), Jin-Feng Jia(贾金锋)
Chin. Phys. B, 2019, 28 (**7**): 077302. DOI: 10.1088/1674-1056/28/7/077302

Quantum oscillations and nontrivial transport in $(Bi_{0.92}In_{0.08})_2Se_3$

Minhao Zhang(张敏昊), Yan Li(李焱), Fengqi Song(宋凤麒), Xuefeng Wang(王学锋), Rong Zhang(张荣)
Chin. Phys. B, 2017, 26 (**12**): 127305. DOI: 10.1088/1674-1056/26/12/127305

Anomalous anisotropic magnetoresistance in single-crystalline Co/$SrTiO_3$(001) heterostructures*

Shuang-Long Yang(杨双龙), De-Zheng Yang(杨德政), Yu Miao(缪宇), Cun-Xu Gao(高存绪), and De-Sheng Xue(薛德胜)†

Key Laboratory for Magnetism and Magnetic Materials of the Ministry of Education, Lanzhou University, Lanzhou 730000, *China*

(Received 3 March 2021; revised manuscript received 29 April 2021; accepted manuscript online 27 May 2021)

The anisotropic magnetoresistances (AMRs) in single crystalline Co(6 nm)/$SrTiO_3$(001) heterostructures from 5 K to 300 K with the current direction setting along either Co[100] or Co[110] are investigated in this work. The anomalous (normal) AMR is observed below (above) 100 K. With the current along Co[100] direction, the AMR shows negative longitudinal and positive transverse magnetoresistances at $T < 100$ K, while the AMR is inverse with the current along Co[110]. Meanwhile, the amplitude ratio between Co[110] and Co[100] is observed to be as large as 29 at 100 K. A crystal symmetry-adapted model of AMR demonstrates that interplay between the non-crystalline component and crossed AMR component results in the anomalous AMR. Our results may reveal more intriguing magneto-transport behaviors of film on $SrTiO_3$ or other perovskite oxides.

Keywords: single crystalline, anisotropic magnetoresistance, heterostructure

PACS: 73.43.Qt, 73.50.–h, 75.47.–m, 75.70.–i **DOI:** 10.1088/1674-1056/ac05ad

1. Introduction

The anisotropic magnetoresistance (AMR) effect, discovered in ferromagnetic metals by Thomson in 1857,[1] is one of the most fundamental characteristics involving magnetic and transport properties[2] and has many practical applications in magnetic recording and sensors.[3] This phenomenon is attributed to spin–orbit coupling which mixes spin-up state with spin-down state,[4–6] and is usually studied in magnetic materials (MMs). While the combined MM with some nonmagnetic materials can form bilayers or multilayers, and thus lots of novel magnetoresistance (MR) phenomena are discovered, such as giant MR in Fe/Cr/Fe,[7] tunneling MR in Fe/MgO/Fe,[8] spin Hall MR (SMR)[9] in ferromagnetic insulator[10,11] or metal,[12] unidirectional SMR[13] in Co/Pt and Co/Ta, Hanle MR in Pt/YIG,[14] anisotropic interface MR in Pt/Co/Pt,[15–17] Rashba–Edelstein MR in Bi/Ag/CoFeB,[18] and spin–orbit MR in Cu[Pt]/$Y_3Fe_5O_{12}$.[19] Although the above MR phenomena originate from different physical essences, they are dependent on spin–orbit coupling and heavily correlated with the nonmagnetic materials or interface.

Interestingly, nonmagnetic oxide $SrTiO_3$ (STO) substrate also has a strong influence on transport properties of a thin film deposited on it. In $LaAlO_3$/STO heterostructures, interfacial Rashba MR,[20] fourfold oscillation AMR and planar Hall effect,[21] as well as giant crystalline AMR[22] were reported.[23–25] Besides these outstanding studies devoted to single crystalline oxides, a few fantastic phenomena in metals/STO heterostructures were realized. In nonmagnetic metallic Al/STO heterostructures, two-dimensional electron gas was formed at room temperature[26] and a very large inverse Edelstein effect[27] was reported. In half-metallic Fe_4N/STO heterostructures, the AMR becomes positive,[28] which is opposed to its natural negative AMR on Si substrate.[29] In addition, more and more studies on AMR have been conducted based on single-crystal magnetic thin films recently, for it can exhibit strong dependence on the current orientation,[30–38] additional four-fold symmetry,[31,34–38] and asymmetric behaviors.[33] However, the signs of above AMR are always positive, and the negative AMR (a fingerprint for half-metallicity[39,40] has never been realized in metallic films. It is interesting to explore whether the single-crystal MM/STO heterostructures show different AMR properties.

In this paper, we study the AMR in the single-crystalline face-centered-cubic (FCC) Co(6 nm)/STO(001) heterostructure as a function of temperature and current direction. The AMR with the current along Co[100] (Co[110]) direction shows anomalous negative (positive) longitudinal MR and positive (negative) transverse MR below 100 K. The anomalous temperature-dependence of the AMR can be well understood by a phenomenological model and attributed to the interplay between the non-crystalline component from the traditional AMR and the crossed AMR component from a mixture of current and crystalline direction related contributions.

2. Experimental details

Co/STO(001) heterostructures were prepared by molecular beam epitaxy in an ultrahigh vacuum chamber with a base

*Project supported by the National Natural Science Foundation of China (Grant Nos. 12174163 and 91963201), the Program for Changjiang Scholars and Innovative Research Team in University, China (Grant No. IRT-16R35), and the 111 Project, China (Grant No. B20063).

†Corresponding author. E-mail: xueds@lzu.edu.cn

© 2021 Chinese Physical Society and IOP Publishing Ltd

pressure better than 4.5×10^{-10} Torr (1 Torr = 1.33322 × 10^2 Pa). The (001)-oriented Co layers were deposited on STO(001) by using thermal evaporator with a substrate temperature held at 400 °C. The Co crystallinity was monitored by *in situ* reflection high-energy electron diffraction (RHEED) during deposition, and further improved by *in situ* annealed at 400 °C for 15 min after deposition. Finally, the heterostructures were covered by a 3-nm-thick Al capping layer to prevent the Co film from oxidizing. High resolution x-ray diffraction (HRXRD) was used to characterize the structure. Magnetic properties were measured with Verslab (Quantum Design). Using standard lithography and Ar-ion etching, the heterostructures were patterned into two Hall bars along Co[100] and Co[110] crystalline directions. The transport properties were performed by using a standard four-probe method with a constant DC current I in a physical property measurement system (quantum design) equipped with a rotatable sample stage. To exclude contributions from the possible misalignment, we did the measurements with both positive and negative field directions.

3. Results and discussion

Figure 1(a) shows the RHEED patterns of Co films and STO substrate with the electron beam along the STO[100] and STO[110] directions, respectively. The elongated stripes of both Co[100] and Co[110] patterns show the formation of an FCC (001) surface. The θ–2θ x-ray diffraction of the 6-nm-thick Co film shown in Fig. 1(b) is consistent with that of the FCC structure. The in-plane lattice parameter calculated from the Co(002) peak is about 3.542 Å. The lattice mismatch between Co and STO[100] (3.905 Å) is 9.3%, which is almost the same as previous result.[41]

Figure 1(c) shows the hysteresis loops measured at room temperature with an in-plane external magnetic field along the Co[100] and Co[110] directions, respectively. The [110] direction as the easy axis (EA) can be clearly seen from the FCC Co film. For the hard-axis loop (H || Co[100]), by applying separate linear fits to the saturated high field and the region between 20 mT and 0 mT, we extract the in-plane magnetocrystalline anisotropy[42,43] of 42.4 mT between the [100] axis and [110] axis. The temperature-dependent zero-field resistivities are depicted in Fig. 1(d) for these two crystalline directions. The resistivities in the two directions decreases clearly with temperature decreasing, as usual. However, the resistivity of I || Co[100] is larger (smaller) than that of I || Co[110] when the temperature is above (below) 150 K. The crystalline direction-dependent resistivity indicates that the MR can be different in the Co[100] direction from in the Co[110] direction.

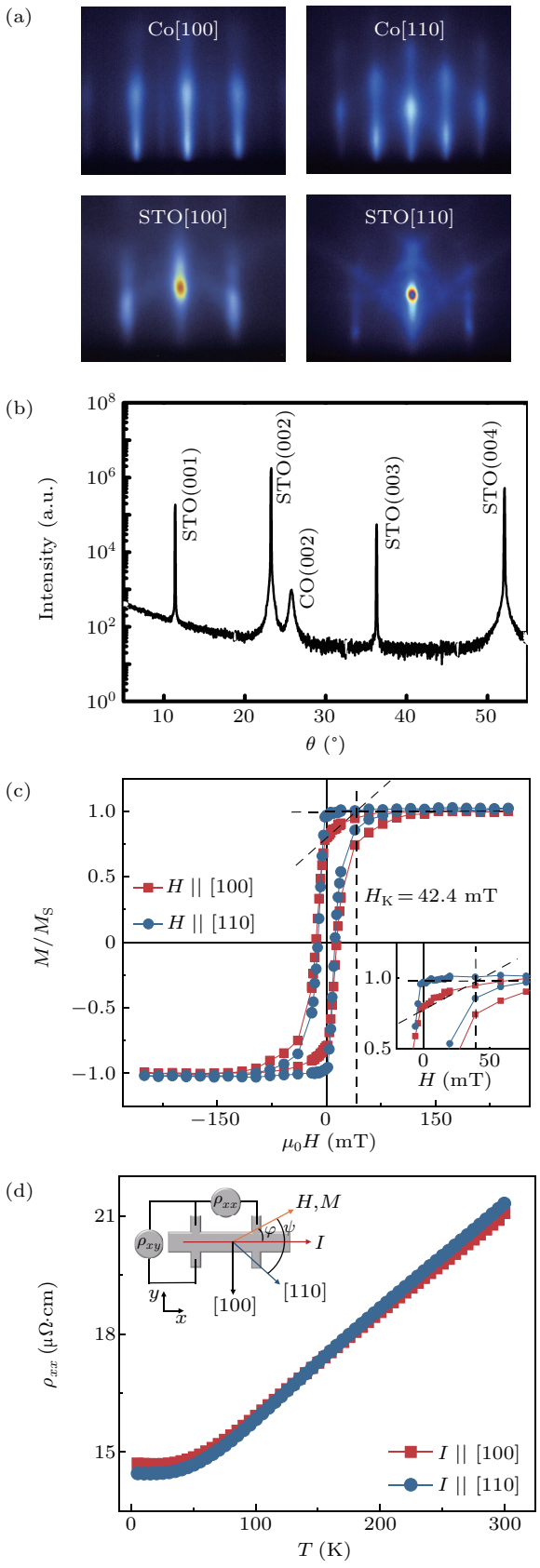


Fig. 1. Characterization results of Co/STO(001) films. (a) RHEED patterns with incident electrons along STO[100] and STO[110] directions. (b) X-ray diffractions (θ–2θ scan). (c) Magnetic hysteresis loop measured at 300 K with magnetic field applied along Co[100] and Co[110] directions. (d) Resistivity ρ_{xx} measured for I || Co[100] and I || Co[110]. The inset shows the sketch of measurement geometry. The unit a.u. is short for arb. units.

The longitudinal resistivity ρ_{xx} measured as a function of magnetic field applied to the film plane for $I \parallel$ Co[100] and $I \parallel$ Co[110] are shown in Fig. 2, where the field parallel and perpendicular to the current. Each of Figs. 2(a) and 2(b) indicates that the field-dependent ρ_{xx} is almost linear and $\rho_{xx}(H \parallel I) > \rho_{xx}(H \perp I)$ for two current directions when the magnetization is saturated at 300 K. However, the results at 5 K shown in Figs. 2(c) and 2(d) display a nonlinear field dependence[42] of ρ_{xx}, $\rho_{xx}(H \parallel I) < \rho_{xx}(H \perp I)$ for $I \parallel$ Co[100] and $\rho_{xx}(H \parallel I) > \rho_{xx}(H \perp I)$ for $I \parallel$ Co[110]. Generally, the resistivity of the current parallel to the magnetization case is larger (smaller) than that of the current perpendicular to the magnetization case, which is defined as the positive (negative) AMR.[2] Hence, the AMRs of two directions are positive, as usual at 300 K, but that at 5 K are negative for $I \parallel$ Co[100] and positive for $I \parallel$ Co[110]. Moreover, the positive or negative AMR is magnetic field-independent after the magnetization has been saturated. In order to clarify the characteristics of AMR, which are heavily dependent on the current direction and temperature, we study the angulardependent AMR further.

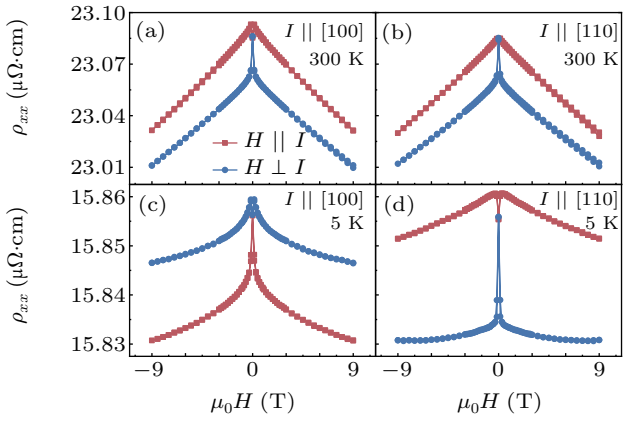


Fig. 2. In-plane MR (MR) curves measured at 300 K and 5 K with $H \parallel I$ and $H \perp I$, with current direction being along [(a), (c)] Co[100] direction and [(b), (d)] Co[110] direction.

Figures 3(a)–3(d) show the AMR curves of Co[100] and Co[110] Hall bars at various temperatures, where $\Delta\rho_{xx} = \rho_{xx} - \rho_{\rm av}$, $\Delta\rho_{xy} = \rho_{xy}$, $\rho_{\rm av}$ is the averaged ρ_{xx} over 360° in plane, and φ is the angle between the external magnetic field and current directions. The field is of constant magnitude 6 T, which is sufficient to saturate the magnetization in plane. Hence, the magnetization is expected to be parallel to the field. The longitudinal AMR curves with current along Co[100] and Co[110] are shown in Figs. 3(a) and 3(b). It is found that the angles where the maximum values located are shifted gradually from $\varphi = 0°$ and 180° at 300 K to nearly $\varphi = 90°$ and 270° at 5 K for the Co[100] Hall bar. However, the AMR observed in Co[110] Hall bar always shows a maximum at $\varphi = 0°$ and 180°. The sign of AMR changes from positive at 300 K to negative at 5 K for Co[100] Hall bar but it is always positive for the Co[110] Hall bar. These results are different from those of the polycrystalline Co,[2,45,46] as well as the single crystalline FCC Co/$LaAlO_3$(001),[30] where the AMR is positive along different directions. Moreover, the current-direction related AMRs reported in FCC Ni/MgO(001), [31] Fe/GaAs,[32,33] and Co_xFe_{1-x}/MgO[34] show an unchanged sign except the symmetry of AMR changing with temperature decreasing. These results demonstrate that the current direction and temperature significantly influence the longitudinal AMR of Co/STO(001) heterostructure.

Furthermore, the transverse AMR is measured and the results are shown in Figs. 3(c) and 3(d). As is well known, the physical origin of traditional longitudinal and transverse AMR[2] are the same, hence, the transverse AMR should have the same corresponding trace as the longitudinal AMR. However, the sign of transverse AMR is changed from positive at 300 K to negative at 5 K for the Co[110] Hall bar, but the transverse AMR is always positive for the Co[100] Hall bar. These results of the transverse AMR never appear in Co,[47,48] Fe/GaAs,[33] or Co_xFe_{1-x}/MgO,[34] which only show the positive behaviors. The different temperature-dependent behaviors of the longitudinal and transverse AMR for two Hall bars enlighten us to consider the contribution of crystal symmetries.

Phenomenologically, a model presented by Rushforth *et al.*[35] according to symmetry,[49] by extending the model of Döring[50] to systems with cubic plus uniaxial anisotropy can be used. As described in this model,[36–38] the longitudinal and transverse AMR both as a function of the angle φ between magnetization $\boldsymbol{M}$ and the in-plane current $\boldsymbol{I}$, and the angle ψ between $\boldsymbol{M}$ and the [110] crystalline direction is written as

$$\begin{aligned} {\rm AMR}_{xx} = \frac{\Delta\rho_{xx}}{\rho_{\rm av}} &= C_{\rm I}\cos 2\varphi + C_{\rm IC}\cos(4\psi - 2\varphi) \\ &\quad + (C_{\rm U}\cos 2\psi + C_{\rm C}\cos 4\psi), \end{aligned} \tag{1}$$

$$ {\rm AMR}_{xy} = \frac{\Delta\rho_{xy}}{\rho_{\rm av}} = C_{\rm I}\sin 2\varphi - C_{\rm IC}\sin(4\psi - 2\varphi), \tag{2}$$

where the coefficients $C_{\rm I}$ and $C_{\rm IC}$ represent the non-crystalline term and the crossed term, $C_{\rm U}$ and $C_{\rm C}$ denote the lowest order uniaxial crystalline term and cubic crystalline term, respectively. For $I \parallel$ Co[100], $\varphi = \psi - 45°$, and for $I \parallel$ Co[110], $\varphi = \psi$. As shown in Fig. 3, the experimental data can be well fitted by the corresponding equations.

Combing Eqs. (1) and (2), the coefficients $C_{\rm I}$, $C_{\rm IC}$, $C_{\rm U}$, and $C_{\rm C}$ obtained by fitting the longitudinal and transverse AMR of $I \parallel$ Co[110] or $I \parallel$ Co[100] are shown in Fig. 4(a). It can be seen that both $C_{\rm I}$ and $C_{\rm IC}$ are larger than $C_{\rm U}$, and $C_{\rm U} > C_{\rm C} \approx 0$. As shown in Eqs. (1) and (2) $(C_{\rm I} - C_{\rm IC})$ terms determine the twofold-symmetry of both the longitudinal AMR in $I \parallel$ Co[100]$(\psi = 45°)$ and transverse AMR in $I \parallel$ Co[110]$(\psi = 0°)$. $C_{\rm I} < C_{\rm IC}$ for $T < 100$ K and $C_{\rm I} > C_{\rm IC}$ for $T \geq 100$ K, and the AMR signs change with temperature decreasing, which are corresponding to Figs. 3(a) and 3(d). Meanwhile, the $C_{\rm U}$ term shifts the longitudinal AMR of $I \parallel$ Co[100]. Similarly, the positive ${\rm AMR}_{xx}$ of $I \parallel$ Co[110] and ${\rm AMR}_{xy}$ of $I \parallel$ Co[100] can also be explained. Clearly, the

non-crystalline term $C_{\rm I}$ and the crossed term $C_{\rm IC}$ are the dominant twofold-symmetric terms, which gives rise to the sign of the AMR, and the twofold-symmetric crystalline term $C_{\rm U}$ slightly change the maximum angle of the AMR curves.

In addition, the strong temperature-dependent AMR amplitudes for the two current directions can be quantitatively elucidated. We plot $\Delta{\rm AMR}_{xx} = {\rm AMR}_{xx}(\varphi = 0^\circ) - {\rm AMR}_{xx}(\varphi = 90^\circ)$ and $\Delta{\rm AMR}_{xy} = {\rm AMR}_{xy}(\varphi = 45^\circ) - {\rm AMR}_{xy}(\varphi = 135^\circ)$ *versus* temperature in Fig. 4(b). $\Delta{\rm AMR}_{xx}$ ($\Delta{\rm AMR}_{xy}$) is small (large) for $I \parallel$ Co[100], and $\Delta{\rm AMR}_{xx}$ ($\Delta{\rm AMR}_{xy}$) is large (small) for $I \parallel$ Co[110]. In addition, $\Delta{\rm AMR}_{xx}$ in $I \parallel$ Co[100] is almost equal to $\Delta{\rm AMR}_{xy}$ in $I \parallel$ Co[110], and *vice versa*. The unambiguously reciprocal relations of AMR amplitudes between the two current directions are coincident with the phenomenological expansions based on symmetry from Eqs. (1) and (2). Furthermore, the ratio $\Delta{\rm AMR}_{xy}^{[100]}/\Delta{\rm AMR}_{xy}^{[110]}$ has a drastic change with temperature and reaches a maximum 29 at 100 K as shown in Fig. 4(c), which is much larger than the other results 1–5.[30–33] Meanwhile, $\Delta{\rm AMR}_{xx}^{[110]}/\Delta{\rm AMR}_{xx}^{[100]}$ has the same dependence on temperature. The large anisotropic dependence on temperature for AMR[37] means that larger ${\rm AMR}_{xx}$ or ${\rm AMR}_{xy}$ can be chosen for designing magnetic sensor or magnetic memory devices with the fixed current direction.

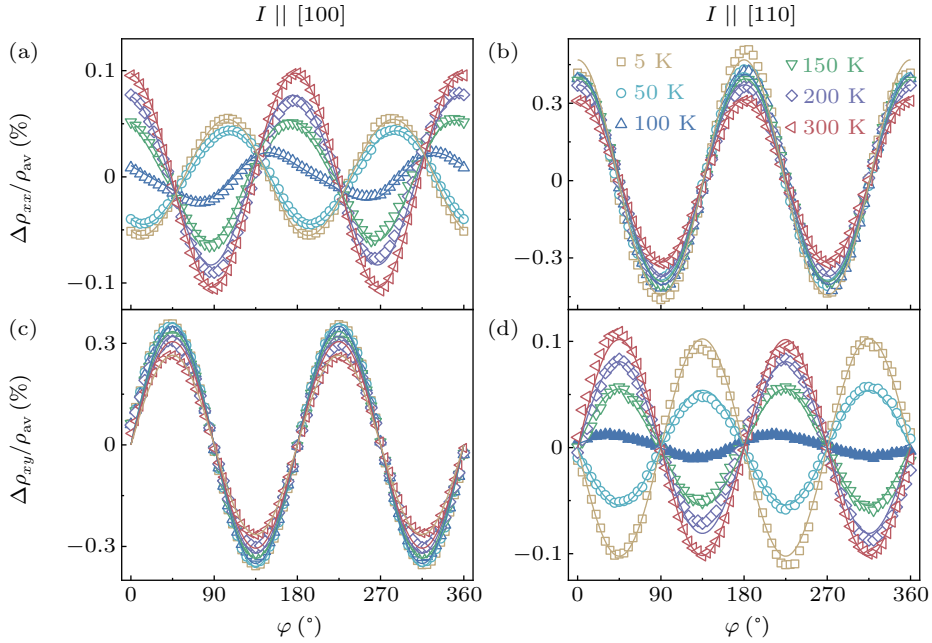


Fig. 3. Curves of in-plane longitudinal and transverse AMR *versus* φ for current along [(a), (c)] Co[100] direction and [(b), (d)] Co[110] direction, with solid linedenoting the experimental data by using Eqs. (1) and (2).

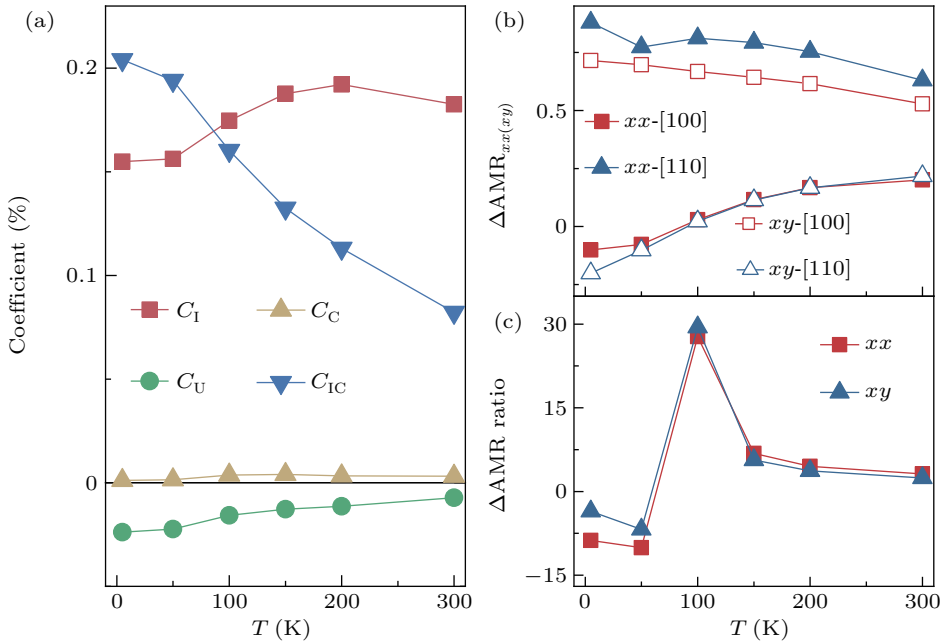


Fig. 4. (a) Curves of fitting coefficients $C_{\rm I}$, $C_{\rm U}$, $C_{\rm C}$, and $C_{\rm IC}$ *versus* temperatures. (b) $\Delta{\rm AMR}_{xx}$ and $\Delta{\rm AMR}_{xy}$ for $I \parallel$ Co[100] and $I \parallel$ Co[110] with decreasing temperature. (c) Amplitude ratio $\Delta{\rm AMR}_{xx}^{[110]}/\Delta{\rm AMR}_{xx}^{[100]}$ (red) and $\Delta{\rm AMR}_{xy}^{[100]}/\Delta{\rm AMR}_{xy}^{[110]}$ (blue) *versus* temperatures.

Furthermore, the AMR under a non-saturated magnetic field is measured, where the magnetization direction is determined by the competition between the applied field and the magnetic anisotropy.[51–54] With 100-mT field, longitudinal AMR of $I \parallel$ Co[110] and transverse AMR of $I \parallel$ Co[100] are obtained in Fig. A1 (Appendix A: Supplementary materials). The fitted cubic (uniaxial) anisotropy field H_K (H_U), and the angle θ_K (θ_U) between the current direction and the easy axis (EA) of cubic (uniaxial) anisotropy field at 300 K are listed in Table 1. The value of H_K is close to 42.4 mT obtained from hysteresis loop in Fig. 1(c). A smaller H_U is along the Co[110] direction, which can be attributed to the in-plane strain induced by the unavoidable miscut on the STO substrate. A similar anisotropy field H_K obtained from magnetic and AMR measurement demonstrates that the AMR may be related to the symmetry of magnetic anisotropy rather than crystalline symmetry.

Table 1. Fitted H_K, H_U, θ_K, θ_U from Fig. A1 at 300 K.

Hall bar	H_K (mT)	θ_K (°)	H_U (mT)	θ_U (°)
AMR-Co[110]	45.2±0.7	1.1±0.1	5.0±2.1	3.1±0.6
PHE-Co[100]	48.2±2.5	48.5±0.7	2.5±1.2	42±3.2

Theoretically, the non-crystalline term C_I depends only on the relative angle between current and magnetization direction. The influence of another dominant term, crossed term C_{IC}, on AMR is studied by varying the thickness of Co. Here, Co(2 nm)/STO and Co(2 nm)/STO heterostructure are measured in a way similar to previous way, and the results are shown in Fig. A2 (Appendix A: Supplementary materials). It is found that the crossed term C_{IC} is larger (smaller) than non-crystalline C_I for Co(2 nm in thickness)(Co(20 nm in thickness)) film. Experimentally, the values of relatively large C_{IC} have been observed for (Ga, Mn) (As, Sb) films,[37] for which the possible reason is the large strain or bulk spin–orbit coupling due to the incorporation of Sb. Further studies indicate that C_{IC} depends on the magnitude (rather than direction) of interfacial spin–orbit field (SOF)[22] as well, while the interfacial SOF induced by the reduced structural symmetry at surfaces and interfaces will be relatively weaken[32] at large thickness. Hence, the anomalous AMR of the Co(6 nm in thickness)/STO heterostructure is closely related to the interface.

4. Conclusion

In this work, the anomalous AMR behaviors in the single-crystalline FCC Co/STO (001) heterostructures are observed. Both the magnitude and the sign of the longitudinal ARM and transverse AMR are dependent on the temperature and the current direction. It is shown that these effects are attributed mainly to the interplay between the non-crystalline component and crossed component. The nature of the anomalous AMR is closely related to the symmetry of magnetic anisotropy and the interface SOF. Our research highlights the significant properties of the Co/STO (001) heterostructures, but more investigations are still required to further clarify the microscopic mechanism behind the magneto-transport behavior in MM/STO system.

Appendix A: Supplementary materials

A1 Magnetic anisotropies determined by magnetoresistance measurements

For the single domain approximation of a single-crystalline film, using the coherent rotation model, the free energy density of the system can be written as[52,53]

$$E = -\mu_0 M_s H \cos(\varphi_H - \varphi_M) + K_u \sin^2(\varphi_M - \theta_u) + \frac{K_c}{4}\sin^2(\varphi_M - \theta_k), \quad \text{(A1)}$$

where μ_0 is the vacuum permeability, M_s is the saturation magnetization, φ_H (φ_M) is the field (magnetization) angle the current direction, K_u (K_c) is the uniaxial (cubic) anisotropy constant, θ_{K_u} (θ_{K_c}) is the angle between uniaxial (cubic) anisotropy and the current direction. $\alpha = \varphi_H - \varphi_M$ can be obtained by $(\partial E)/(\partial \alpha) = 0$ with small angle approximation

$$\varphi_M \approx \varphi_H - \frac{2h_2 \sin 2(\varphi_H - \theta_u) + \sin 4(\varphi_H - \theta_k)}{4h_1 + 4h_2 \cos 2(\varphi_H - \theta_u) + 4\cos 4(\varphi_H - \theta_k)}, \quad \text{(A2)}$$

where $h_1 = H/H_k$, $h_2 = H_u/H_k$, H_k and H_u are the effective cubic and uniaxial anisotropy fields. The ϕ_M can be determined by the angledependent magnetoresistance measurement. Hence, combining Eq. (A2) with Eq. (1) or Eq. (2) in the main text, H_k, H_u, θ_k, θ_u can be quantified by fitting the magnetoresistance curve.

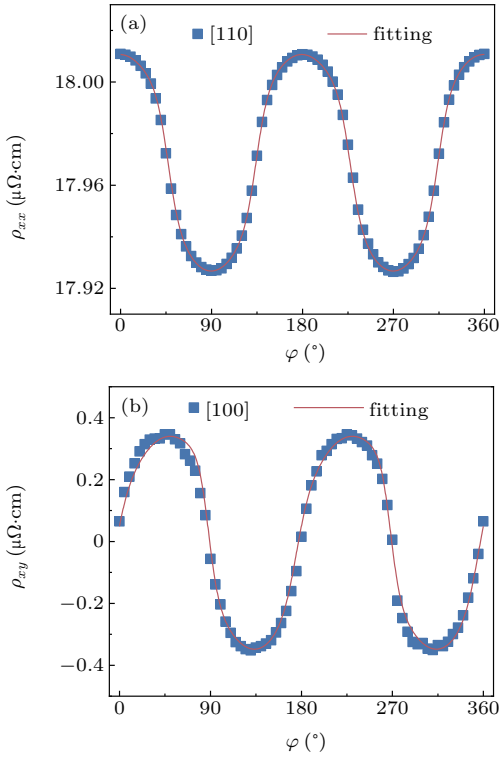


Fig. A1. (a) Longitudinal magnetoresistance for $I \parallel$ Co[110] and fitted by combining Eq. (A2) with Eq. (1). (b) Transverse magnetoresistance for $I \parallel$ Co[100] and fitted by combining Eq. (A2) with Eq. (2).

Figures A1(a) and A1(b) show longitudinal magnetoresistance for $I \parallel$ Co[110] and transverse magnetoresistance for $I \parallel$ Co[100] with $H = 100$ mT at 300 K. The fitted results are shown in Table 1 of the main text.

A2 Magnetoresistance in Co(2 nm)/STO(001) and Co(20 nm)/STO(001)

Co(2 nm)/STO(001) and Co(20 nm)/STO(001) films are prepared and measured in a way similarto previous way and the coefficients fitted with the above phenomenological model are shown in Fig. A2. The non-crystalline term and the crossed term are the dominant terms similar to the Co (6 nm)/STO, but non-crystalline term is clearly smaller (larger) than the crossed term over the whole temperature range in Co(2 nm)/STO(001) (Co(20 nm)/STO(001)).

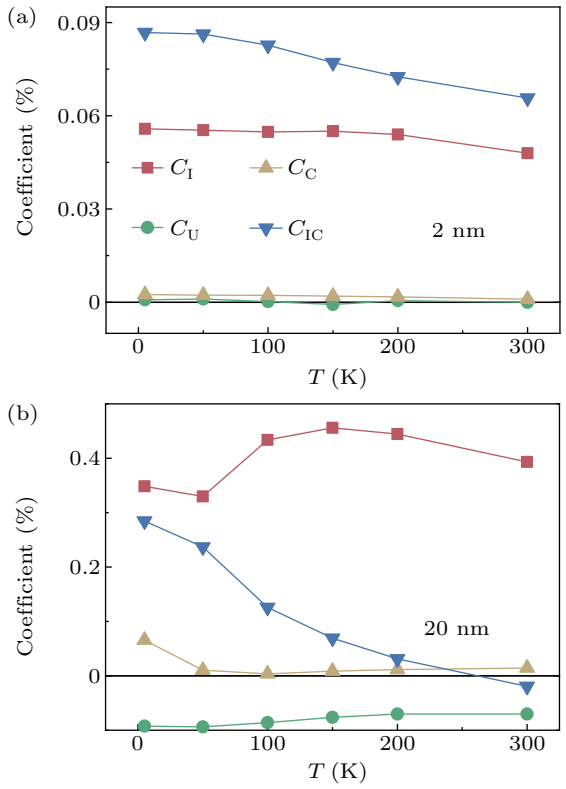


Fig. A2. Curves of fitted AMR coefficients C_I, C_U, C_C, and C_{IC} *versus* temperature of (a) Co(2 nm) and (b) Co(20 nm) , respectively .

References

[1] Thomson W 1857 *Proc. R. Soc.* 546

[2] McGuire T and Potter R 1975 *IEEE Trans. Magn.* **11** 1018

[3] Li J, Jin E, Son H, Tan A, Cao W N, Hwang C and Qiu Z Q 2012 *Rev. Sci. Instrum.* **83** 033906

[4] Campbell I A, Fert A and Jaoul O 1970 *J. Magn. Magn. Mater.* **3** S95

[5] Smit J 1951 *Physica* **17** 612

[6] Berger L 1963 *J. Appl. Phys.* **34** 1360

[7] Baibich M N, Broto J M, Fert A, Van Dau F N, Petroff F, Etienne P, Creuzet G, Friederich A and Chazelas J 1988 *Phys. Rev. Lett.* **61** 2472

[8] Yuasa S, Nagahama T, Fukushima A, Suzuki Y and Ando K 2005 *Nat. Mater.* **3** 868

[9] Chen Y T, Takahashi S, Nakayama H, Althammer M, Goennenwein S T B, Saitoh E and Bauer G E W 2013 *Phys. Rev. B* **87** 144411

[10] Nakayama H, Althammer M, Chen Y T, Uchida K, Kajiwara Y, Kikuchi D, Ohtani T, Geprägs S, Opel M, Takahashi S, Gross R, Bauer G E W, Goennenwein S T B and Saitoh E 2013 *Phys. Rev. Lett.* **110** 206601

[11] Miao B F, Huang S Y, Qu D and Chien C L 2014 *Phys. Rev. Lett.* **112** 236601

[12] Kim J, Sheng P, Takahashi S, Mitani S and Hayashi M 2016 *Phys. Rev. Lett.* **116** 097201

[13] Avci C O, Garello K, Ghosh A, Gabureac M, Alvarado S F and Gambardella P 2015 *Nat. Phys.* **11** 570

[14] Vélez S, Golovach V N, Bedoya-Pinto A, Isasa M, Sagasta E, Abadia M, Rogero C, Hueso L E, Bergeret F S and Casanova F 2016 *Phys. Rev. Lett.* **116** 016603

[15] Kobs A, Heße S, Kreuzpaintner W, Winkler G, Lott D, Weinberger P, Schreyer A and Oepen H P 2011 *Phys. Rev. Lett.* **106** 217207

[16] Kobs A, Heße S, Oepen H and Weinberger P 2012 *Philos. Mag.* **92** 2835

[17] Kobs A, Frauen A and Oepen H P 2014 *Phys. Rev. B* **90** 016401

[18] Nakayama H, Kanno Y, An H, Tashiro T, Haku S, Nomura A and Ando K 2016 *Phys. Rev. Lett.* **117** 116602

[19] Zhou L, Song H, Liu K *et al.* 2018 *Sci. Adv.* **4** eaao3318

[20] Narayanapillai K, Go G, Ramaswamy R, Gopinadhan K, Go D, Lee H W, Venkatesan T, Lee K J and Yang H 2017 *Phys. Rev. B* **96** 064401

[21] Annadi A, Huang Z, Gopinadhan K, Wang X R, Srivastava A, Liu Z Q, Ma H H, Sarkar T P, Venkatesan T and Ariando 2013 *Phys. Rev. B* **87** 201102

[22] Ma H J H, Zhou J, Yang M, Liu Y, Zeng S W, Zhou W X, Zhang L C, Venkatesan T, Feng Y P and Ariando 2017 *Phys. Rev. B* **95** 155314

[23] Ben Shalom M, Tai C W, Lereah Y, Sachs M, Levy E, Rakhmilevitch D, Palevski A and Dagan Y 2009 *Phys. Rev. B* **80** 140403

[24] Flekser E, Ben Shalom M, Kim M, Bell C, Hikita Y, Hwang H Y and Dagan Y 2012 *Phys. Rev. B* **86** 121104

[25] Yang H, Zhang B, Zhang X, Yan X, Cai W, Zhao Y, Sun J, Wang K L, Zhu D and Zhao W 2019 *Phys. Rev. Appl.* **12** 034004

[26] Rödel T C, Fortuna F, Sengupta S, Frantzeskakis E, Fèvre P L, Bertran F, Mercey B, Matzen S, Agnus G, Maroutian T, Lecoeur P and Santander-Syro A F 2016 *Adv. Mater.* **28** 1976

[27] D C Vaz P Noël A J B G F Y B G S S M W F T L M V A and A Sander N M 2019 *Nat. Mater.* **18** 1976

[28] Nikolaev K R, Krivorotov I N, Dahlberg E D, Vas'ko V A, Urazhdin S, Loloee R and Pratt W P 2003 *Appl. Phys. Lett.* **82** 4534

[29] Tsunoda M, Komasaki Y, Kokado S, Isogami S, Chen C C and Takahashi M 2009 *Appl. Phys. Express* **2** 083001

[30] Xiao X, Liang J H, Chen B L, Li J X, Ma D H, Ding Z and Wu Y Z 2015 *J. Appl. Phys.* **118** 043908

[31] Xiao X, Li J X, Ding Z and Wu Y Z 2015 *J. Appl. Phys.* **118** 203905

[32] Hupfauer T, Matos-Abiague A, Gmitra M, Schiller F, Loher J, Bougeard D, Back C H, Fabian J and Weiss D 2015 *Nat. Commun.* **6**

[33] Zeng F L, Zhou C, Jia M W, Shi D and Wu Y Z 2019 *J. Magn. Magn. Mater.* **499** 166204

[34] Zeng F L, Ren Z Y, Li Y, Zeng J Y, Jia M W, Miao J, Hoffmann A, Zhang W, Wu Y Z and Yuan Z 2020 *Phys. Rev. Lett.* **125** 097201

[35] Rushforth A W, Výborný K, King C S, Edmonds K W, Campion R P, Foxon C T, Wunderlich J, Irvine A C, Vaek P, Novák V, Olejník K, Sinova J, Jungwirth T and Gallagher B L 2007 *Phys. Rev. Lett.* **99** 147207

[36] Rushforth A W, Výborný K, King C S, Edmonds K W, Campion R P, Foxon C T, Wunderlich J, Irvine A C, Novák V and Olejník K 2009 *J. Magn. Magn. Mater.* **321** 1001

[37] Howells B, Wang M, Edmonds K W, Wadley P, Campion R P, Rushforth A W, Foxon C T and Gallagher B L 2013 *Appl. Phys. Lett.* **102** 052407

[38] Ranieri E D, Rushforth A W, Výborný K, Rana U, Ahmad E, Campion R P, Foxon C T, Gallagher B L, Irvine A C, Wunderlich J and Jungwirth T 2008 *New J. Appl. Phys.* **10** 065003

[39] Yang F J, Sakuraba Y, Kokado S, Kota Y, Sakuma A and Takanashi K 2012 *Phys. Rev. B* **86** 020409

[40] Kokado S, Tsunoda M, Harigaya K and Sakuma A 2012 *J. Phys. Soc. Jpn.* **81** 024705

[41] Yabuhara O, Nukaga Y, Ohtake M, Kirino F and Futamoto M 2010 *J. Magn. Soc. Jpn.* **34** 78
[42] Kittel C 1996 *Introduction to Solid State Physics* (Wiley)
[43] Lee A J, Brangham J T, Cheng Y, White S P, Ruane W T, Esser B D, McComb D W, Hammel P C and Yang F Y 2017 *Nat. Commun.* **8** 234
[44] Raquet B, Viret M, Sondergard E, Cespedes O and Mamy R 2002 *Phys. Rev. B* **66** 024433
[45] Freitas P, Gomes A, McGuire T and Plaskett T 1990 *J. Magn. Magn. Mater.* **83** 113
[46] Gil W, Görlitz D, Horisberger M and Kötzler J 2005 *Phys. Rev. B* **72** 134401
[47] Epshtein E M, Krikunov A I and F Y 2003 *J. Magn. Magn. Mater.* **258–259** 80
[48] Lima S C and Baibich M N 2016 *J. Appl. Phys.* **119** 033902
[49] Birss R R *et al.* 1964 *Symmetry and Magnetism*, Vol. 863 (North-Holland Amsterdam)
[50] Döring W 1938 *Ann. Phys.* **424** 259
[51] Cao W N, Li J, Chen G, Zhu J, Hu C R and Wu Y Z 2011 *Appl. Phys. Lett.* **98** 262506
[52] Miao Y, Chen X, Yang S, Zheng K, Lian Z, Wang Y, Wang P, Gao C, Yang D Z and Xue D S 2020 *J. Magn. Magn. Mater.* **512** 167013
[53] Qeemat G, He W, Li Y, Sun R, Li N, Yang X, Li Y, Gong Z Z, Xie Z, Zhang X, Cheng Z H 2018 *Chin. Phys. B* **27** 097504
[54] Syed S A, He W, Tang J, Zhang S, Hu B, Ye J, Gul Q, Zhang X and Cheng Z H 2016 *Chin. Phys. B* **25** 097501
[55] Cao W N, Li J, Chen G, Zhu J, Hu C R and Wu Y Z 2011 *Appl. Phys. Lett.* **98** 1413